16 Impact of Upgrade on ZEUS Detector Performance

This chapter presents a summary of a study of the impact of the new IP on the performance of the ZEUS detector, see [1] and [2] for more details. In particular the effect of the dead material introduced by the new magnets and necessary synchrotron radiation absorbers has been studied by incorporating the main features of the designs into the ZEUS detector simulation program (MOZART). The study was done for the IP with normal conducting magnets (**Rev1**). It will be repeated for the superconducting magnets (**Rev2**).

16.1 Description of the interaction region within the ZEUS MC

The upgrade Monte Carlo (MC) simulation was based on the 1994 version of MOZART (Num12vB). This has almost the correct geometry for both the FCAL and RCAL (the RCAL is horizontally offset by 1 cm in 1994, compared to 1.5 cm proposed for the upgrade).

Three modifications to the 1994 geometry were then made:

- Replacement of the "dead-material" (i.e. beam pipe, absorbers, collimators and read out cables) from the back of the FCAL through to the back of the RCAL (MOZART volume FPIP, PIPE and RPIP). No attempt was made to model any changes past the end of the calorimeter.
- Modification of the magnetic field due to the new magnets; this was implemented very simply. A uniform vertical field $B_y = 0.15\,\mathrm{T}$ was added to the existing field for tracking inside the magnet volumes.
- A simple description of the micro vertex detector (μVD) was also provided, with 3 Si barrels and 4 forward Si planes of appropriate thickness. MC energy deposits in the silicon were read out to the VCHIT table.

The geometry of the new magnets and beam pipe was described very simply. The rather complicated shape of the combined function magnet (CFM) was reduced to a copper block of cross-section $15\,\mathrm{cm} \times 15\,\mathrm{cm}$; the density of the copper was reduced to $\rho = 6\,\mathrm{gcm}^{-3}$ which represents the mean density of material in that region. The absorption and radiations lengths of the copper were increased correspondingly. The copper coil heads were represented using a smaller block of full density copper.

The beam-pipe was formed from 3 mm thick aluminium pieces, except for the very central region inside the μVD, which was made from 1.5 mm thick carbon fibre. Various aluminium and steel flanges were implemented as specified in the technical drawings of the upgrade (figures 96 and 44). To protect the detector from the fan of synchrotron radiation, tungsten absorbers were positioned at $z = 137$ cm and $z = -81$ cm. The xz view of the central beam pipe region as implemented in MOZART for this upgrade design is shown in figure 97.

As discussed in later sections, this design produced a large amount of scattering in the forward CFM resulting in a large increase in the number of FDET hits and the FCAL energy. These results motivated two separate design changes which were also implemented in the Monte Carlo:

- the forward CFM was shortened by 10 cm and moved by $z = +20$ cm away from the interaction region;

- the forward and rear CFM were shortened such that the forward CFM is flush with the face of the FCAL at $z = 220$ cm as shown in figure 98. The additional required bending power is produced by permanent cobalt-samarium (CoSm) magnets. These were implemented in GEANT as cylinders of pure cobalt, with an inner radius of 40 mm and a thickness of 5 mm. The 15 mm thick cylindrical aluminium support structure was also described. The cylindrical shape represents a simplification of the true octagonal shape of the CoSm magnets, but the difference was felt to be unimportant for the simulation.

16.2 Impact on components

16.3 Forward tracking detector

The influence of the three upgrade designs has been checked using a neutral current DIS Monte Carlo sample with $Q^2 > 10$ GeV^2. In figure **??** the mean number of hits, LTEs and segments in the 3 chambers are compared. There are only small differences in FTD1 (layers 1-3), but in FTD3 (layers 7-9) the number of hits is increased by a factor of two, and 20% more segments are found for the first upgrade design. Although there is much more activity in FTD3, it seems that most of the hits produced by scattered particles are removed in the segment reconstruction. For the latest upgrade design where the CFM is shortened and flush with the face of the FCAL the activity in FTD3 is significantly decreased. We observe nearly the same number of segments as in the case with no magnet.

16.4 Central tracking detector

A study was made for the tracks found and for the tracks assigned to the primary vertex ,comparing the 1994 detector simulation and the upgrade design with the long CFM. In general the upgrade has little effect on the distributions except for events with high track multiplicity where more high multiplicity events are observed. The same feature is present for the CoSm upgrade design.

16.5 Calorimeter

The effect of the upgrade on the calorimeter energy spectrum was considered for all three upgrade designs using DIS events with $Q^2 > 10$ GeV^2. Figure 99 shows that on average 20-30 GeV of additional energy is seen in the FCAL after the upgrade. The design with the shortest CFMs and CoSm magnets has the largest effect.

Although most of the excess energy seen in the calorimeter is in the FCAL, there is also on average a 0.5-1.5 GeV increase in the BCAL energy. This effect is the most serious for the upgrade design with long CFMs, and improves as the magnet is made shorter.

The difference in the RCAL energy spectrum in figure **??** is attributed to the VXD cables which are present in the 1994 detector configuration but removed in the upgrade simulations.

To investigate if the extra energy in the FCAL is confined to the cells surrounding the beam pipe, the total energy in the FCAL cells excluding those in the inner and inner two rings in the three upgrade designs is compared to the standard detector simulation. Better agreement between the upgrade designs and the current detector is observed when the cells in the two inner rings are excluded, however there is still a factor of up to three difference between the long CFM design and the Num12vB spectrum while the design with the shortest CFMs and CoSm magnets deviates least from the Num12vB simulation.

Figure 100 shows the FCAL energy distribution for DIS MC with $Q^2 > 1000$ GeV^2 . The upgrade presents less of a problem for medium and high Q^2 (high x) events where the current jet is in the forward direction. Then the amount of FCAL energy associated with the primary interaction is large compared to the FCAL energy resulting from secondary interactions in the magnets.

16.6 Leading proton spectrometer

Any changes in the straight-section optics immediately implies changes in the LPS and the aim has been to keep the resultant modifications and expenses to a minimum. In ZEUS Note 96-087 a study was made with partial information about the beam. Since then, the HERA optics design has been modified and extended so that beta functions match their previous values after 60 m from the interaction point. An important result of this is that the LPS stations S4, S5 and S6 will remain unchanged. Before S4, the beam is different and that part of the spectrometer has been re-designed. The optimal station positions are shown on the optical-function drawing of the beam in fig. 101. Acceptances (fig. 102) have been calculated assuming a coincidence selection $(S1.S2)$ OR $(\geq 2$ $from$ $S3$ $S4$ $S5$ $S6)$, though the contribution from $S3$ is quite small.

The highest acceptance is obtained if the shapes of the detectors in $S1$ and $S2$ are modified and also the coil winding in one quadrant of the preceding $QJ2B$ septum-quadrupole is modified to allow a wider vacuum vessel. The feasibility and details of the vacuum vessel modification will be studied as part of the next phase of the HERA update design and this and any modifications to the beam resulting from the conclusions of this study group will influence the LPS design, so the conclusions of this note may change.

16.7 Electron-finding in DIS

One of the major motivations for the luminosity upgrade is to extend the kinematic region over which DIS measurements can be made to very high values of Q^2. Electron-finding will be important for a wide range of exotic physics signatures as well as NC DIS measurements.

To determine whether the increase in FCAL energy would have a detrimental effect on high Q^2 electron-finding, medium ($Q^2 > 1000$ GeV^2) and high ($Q^2 > 20000$ GeV^2) NC DIS Monte Carlo events were used to study the efficiency of the Sinistra electron finder. While this electron finder has not been tuned to provide a high efficiency in this kinematic region, it was felt that the results would give an indication of the impact of the upgrade on electron identification.

The electron-finding efficiency (based on CAL information only) is greater than 90% for electrons in the BCAL. For $\theta_e > 0.4$ rads, the electron finding efficiency is not affected by the upgrade. For very forward electrons with $\theta < 0.3$ radians however, there is a significant loss in efficiency, $\sim 10 - 15\%$, after the upgrade.

In more detail, using the very forward and very high energy electrons ($E_e > 200$ GeV) in NC DIS events with $Q^2 > 20,000$ GeV^2 ,it is seen that the purity of the electron finder does not degrade by more than 4% in the very forward region.

Further,the angular distributions of the reconstructed electrons before and after the upgrade are compared. The electron isolation is measured in terms of E_{cone}, the summed energy of calorimeter cells in an $\eta - \phi$ cone of radius 0.8 around the electron direction, excluding those associated with the electron. In general, the upgrade has little effect on the measured electron quantities. The largest discrepancy in the energy spectrum in is due to the removal of the VXD cables in the upgrade simulations.

16.8 Neutral current reconstruction

In the range $0.08 < y < 0.9$, there is a good agreement between the long CFM upgrade and 1994 simulations. However for the CFM and CoSm design the y resolution degrades by $\sim 10\%$ in this range. At very low values of $y < 0.01$ where the hadronic system is at very forward angles the increase in extra FCAL energy causes the relative pull in y_{JB} to increase from 1.6 to 2.6-3.

16.9 Transverse energy flows in NC DIS

The transverse hadronic energy flow has been measured in the laboratory frame for DIS events with $10 < Q^2 < 7500$ GeV^2. The impact of the upgrade has been quantified in terms of the ratio of reconstructed/generated E_T flow. This is the inverse of the bin-by-bin correction function that may be applied to data in such an analysis. It is therefore desirable that this ratio does not deviate from 1 by a significant amount.

The reconstructed/generated energy flow ratio for the current detector layout and the long CFM upgrade design were compared. For $\eta > 1$, this ratio increases by a factor of two as a direct consequence of the extra FCAL energy observed in section 16.5. The same effect is observed in different Q^2 and W ranges.

16.10 Jet-finding in NC DIS

The effects of the upgrade magnets on the measurement of inclusive jets have been studied in NC DIS events at relatively low $Q^2 > 10$ GeV^2. Such measurements are of particular concern for many physics topics, such as searches for BFKL effects.

The jets were found using the k_T algorithm applied in the laboratory frame and were then boosted to the Breit frame to investigate their properties.

There is a large increase in the number of jets found for the long CFM upgrade design compared to the current configuration in the region $\eta^* > 1.5$. Moreover, on average 43 more calorimeter cells are used as input to the jet algorithm in the upgrade configuration compared to the standard one.

Another measure is the ratio of the η^*(cells)/η^*(hadrons). This is the inverse of the factor needed to correct the jets found at the detector level back to the hadron level. A very large increase in this ratio is observed for jets with $\eta^* > 1.5$ for the upgrade compared.

16.11 Charged current reconstruction

The study shows, that no significant effect of the HERA upgrade on CC DIS measurements at ZEUS is present. However more detailed studies are needed to verify the possible influence on selection criteria, efficiencies, etc.

16.12 Jet-finding in photoproduction

With the advent of the upgrade (long CFM design), there were 28% more jets observed in the calorimeter from the photoproduction sample.

In general,large effects of the upgrade were observed. While the design with shorter CFM with CoSm magnets represents an improvement over the design with long combined-function magnets, the effects shown in both cases are significant. The changes are larger than those seen in the previous study for a different magnet design. The events used then - for the photoproduction study - were of the same type, but the differences in 'resolution' were less marked. Consequently the analysis of jet quantities in photoproduction would be greatly impaired. This would be particularly drastic in the forward region and consequently could lead to jet analyses being performed over a narrower range in η.

16.13 Conclusions

The HERA upgrade is predicted to increase the specific luminosity by a factor of $\sim$4 relative to the 1995 value. However, introducing magnets with a small inner-diameter into the interaction region causes a significant impact on components in the forward region, most notably the FCAL and the FDET due to particle-showering in the magnets. This impairs the measurement of forward jets and would therefore restrict the η range over which jet analyses in both DIS and photoproduction could be performed. The electron-finding efficiency for very forward electrons is also degraded as a consequence, however, it may be possible to improve the efficiency by re-tuning the electron-finding algorithm. Analyses based on tracks in the CTD and charged current reconstruction do not suffer.

Three separate magnet designs **Rev1** have been considered, the one with the long combined function magnets being the technically preferred solution. While it has the largest impact on the FDET and calorimeter energy measurements beyond the two inner rings, the other designs remain problematic.

The impact on the FCAL and FDET measurements is expected to be less severe for the IP with superconducting magnets **Rev2**, because of the increased inner radius and significantly less material of the coil compared to the normal conducting version. The MC study will be repeated for the superconducting magnets.

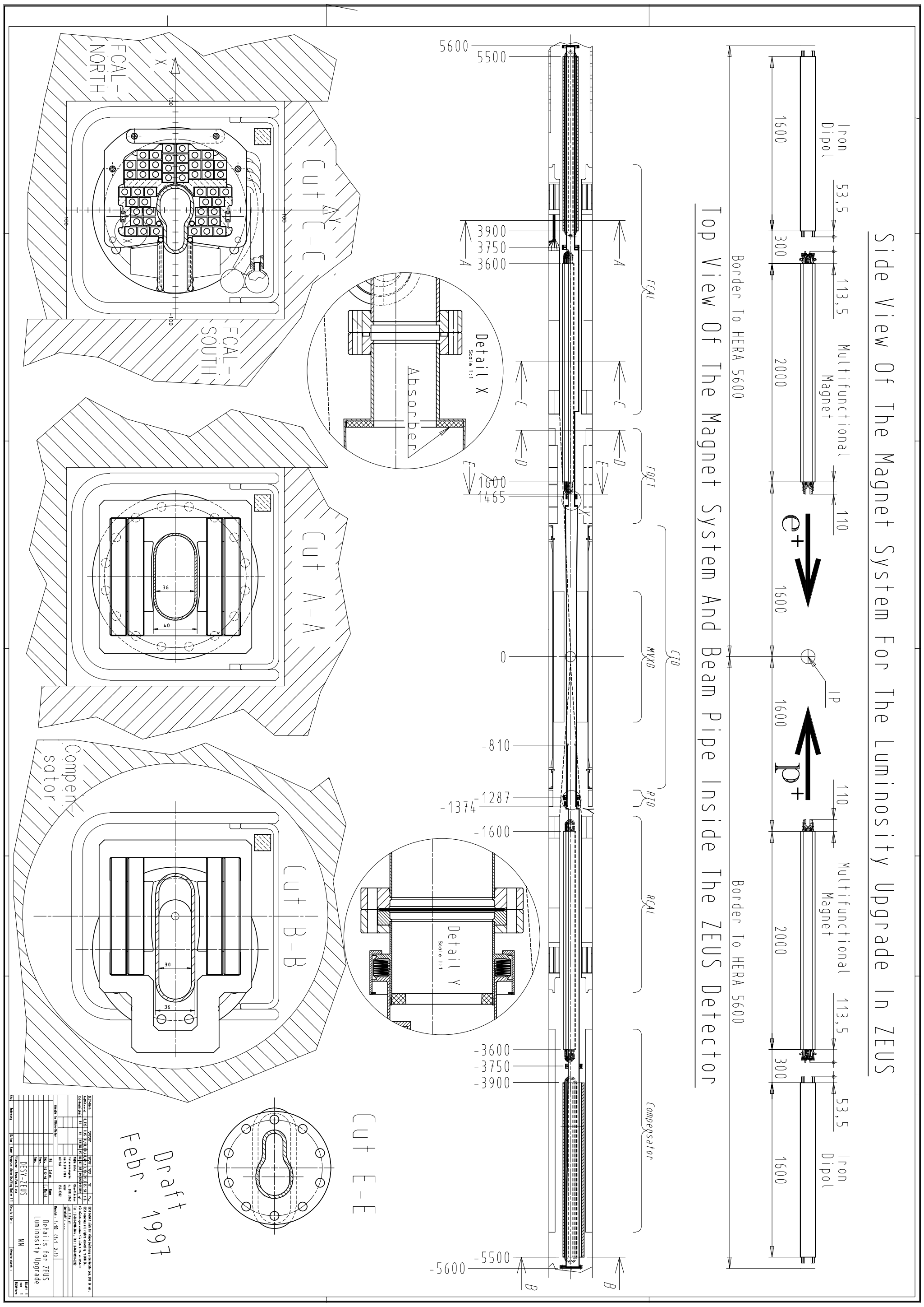

Figure 96: Technical drawing of the new ZEUS interaction region and beam line.

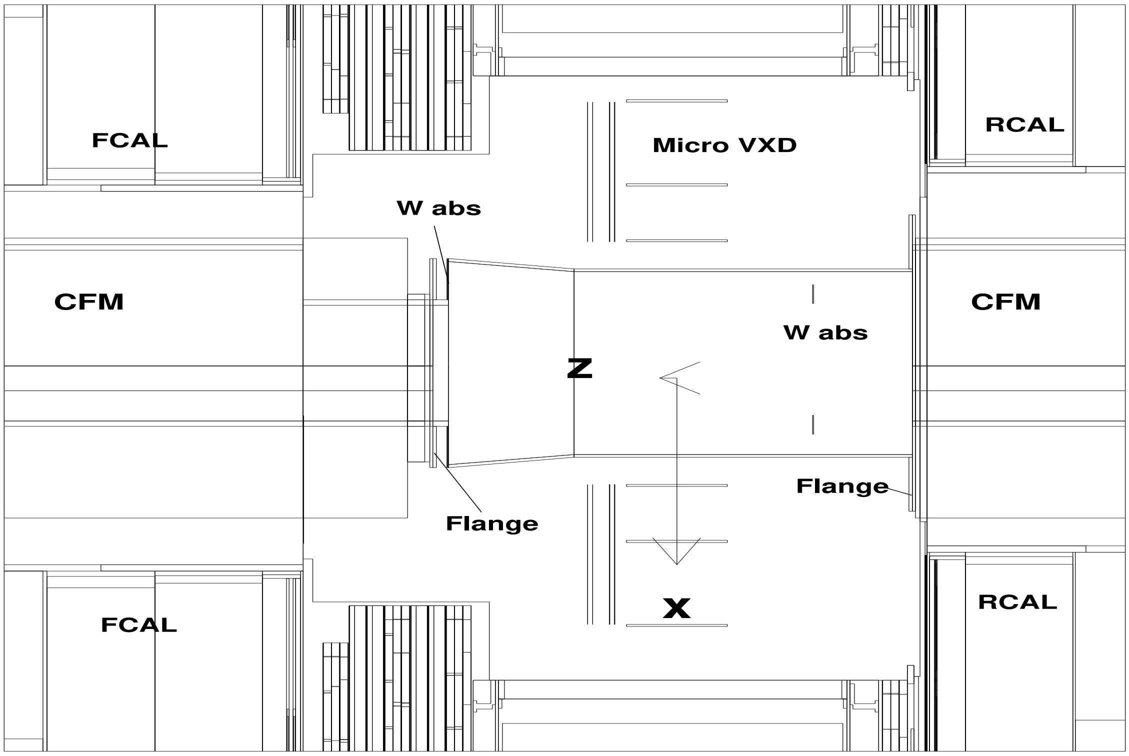

Figure 97: An XZ (top) view of the central beam pipe region of upgrade design 1. The new beam pipe and long CFMs can be seen, as well as the barrel and forward plane μVXD volumes. Note the greatly expanded X scale relative to the Z scale.

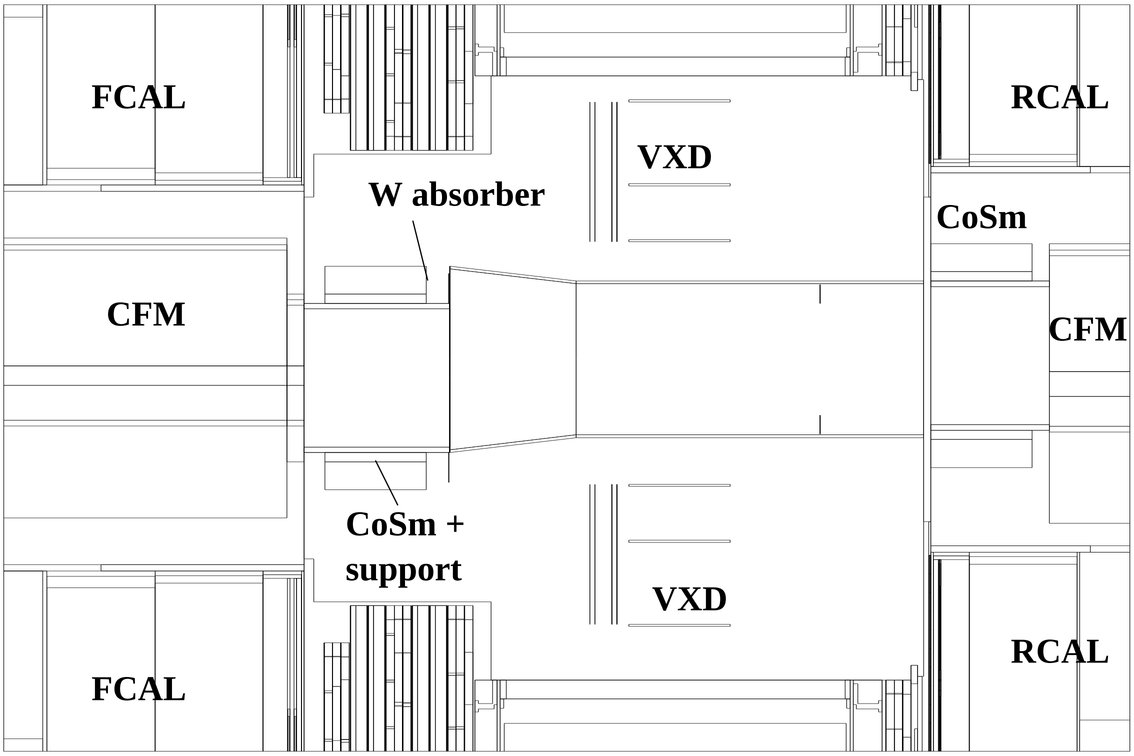

Figure 98: An XZ (top) view of the central beam pipe region of upgrade design 3.

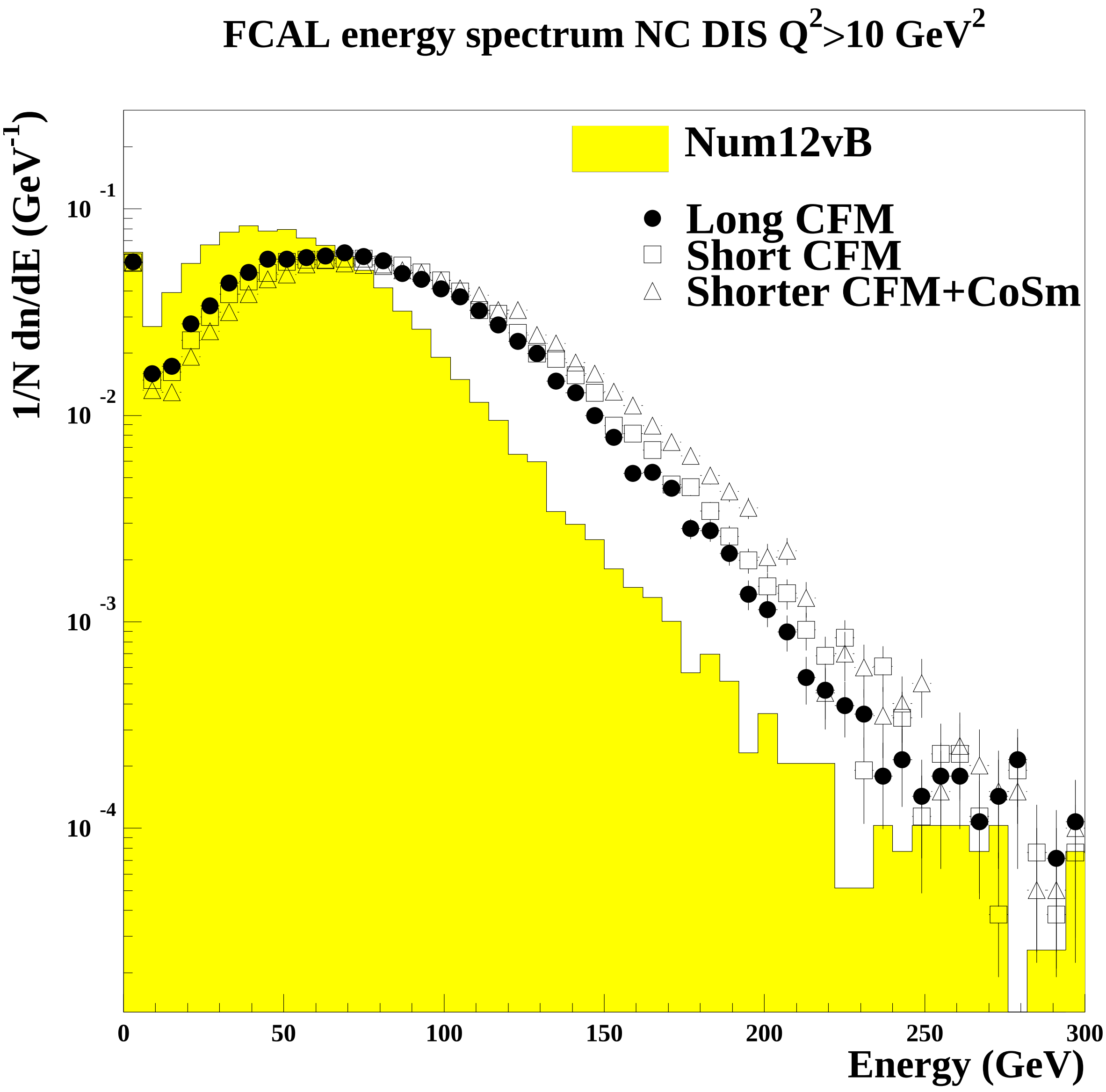

Figure 99: FCAL energy spectrum in NC DIS events with $Q^2 > 10$ GeV^2.

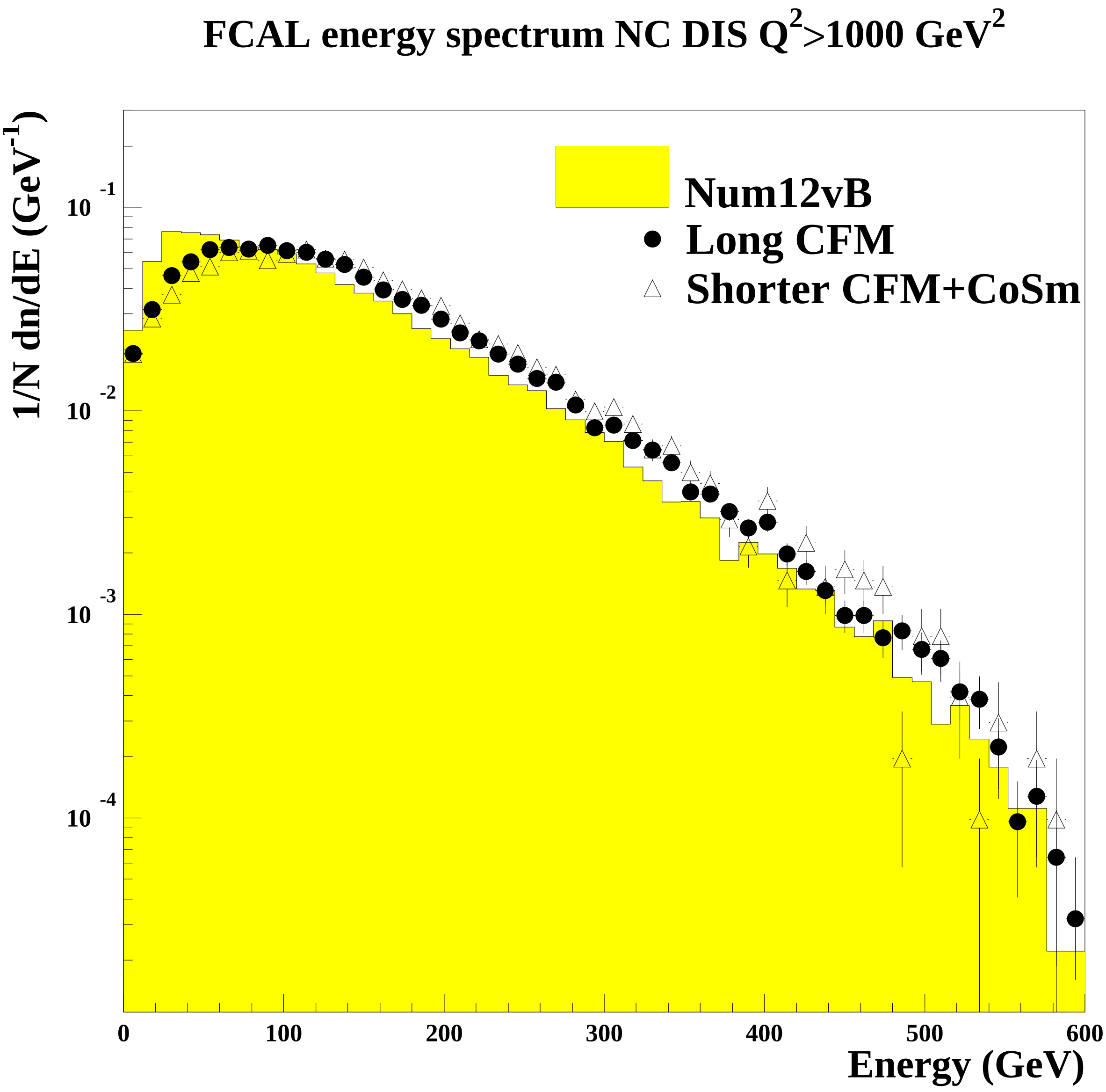

Figure 100: Energy distribution in the FCAL for $Q^2 > 1000\ \mathrm{GeV}^2$ DIS events.

References

[1] V.A. Noyes (ed.), ZEUS Note 97-035 (1997).

[2] T. Massam, ZEUS Note 97-038 (1997).

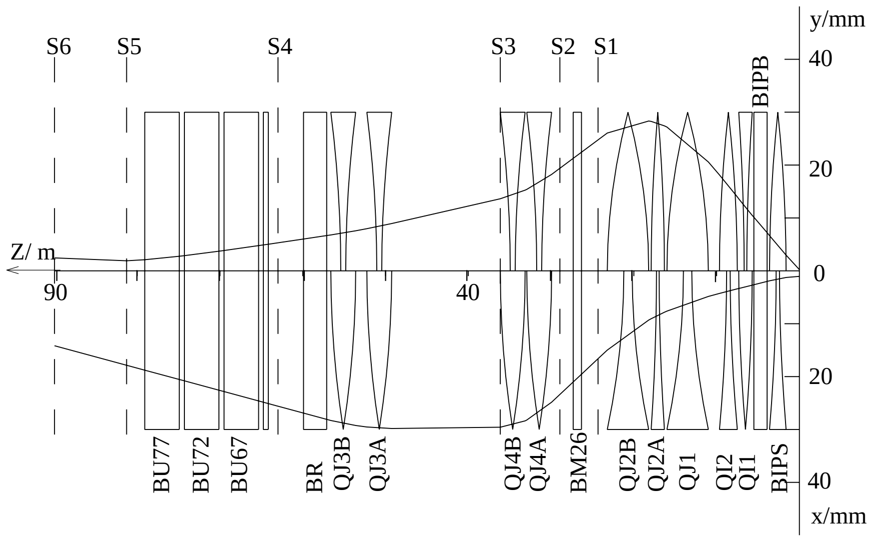

Figure 101: Horizontal and vertical optical layout of the beam in the LPS. Electron magnets: $BIPS$ combined function; $BIPB$ bending; $QI1$, $QI2$ low-beta quadrupoles. Proton magnets: $QJ1$ (magnetic septum) and $QJ2A, B$ (current septum) low beta quadrupoles; $QJ2$, $QJ2$ conventional quadrupoles to match the phase space to its previous shape at $z = 60\,m$. BM and BR bending magnets steer the beam onto its original orbit. Vacuum vessel shapes have not yet been designed. Reasonable design assumptions based on the the expected coil and pole layouts have been made for this study.

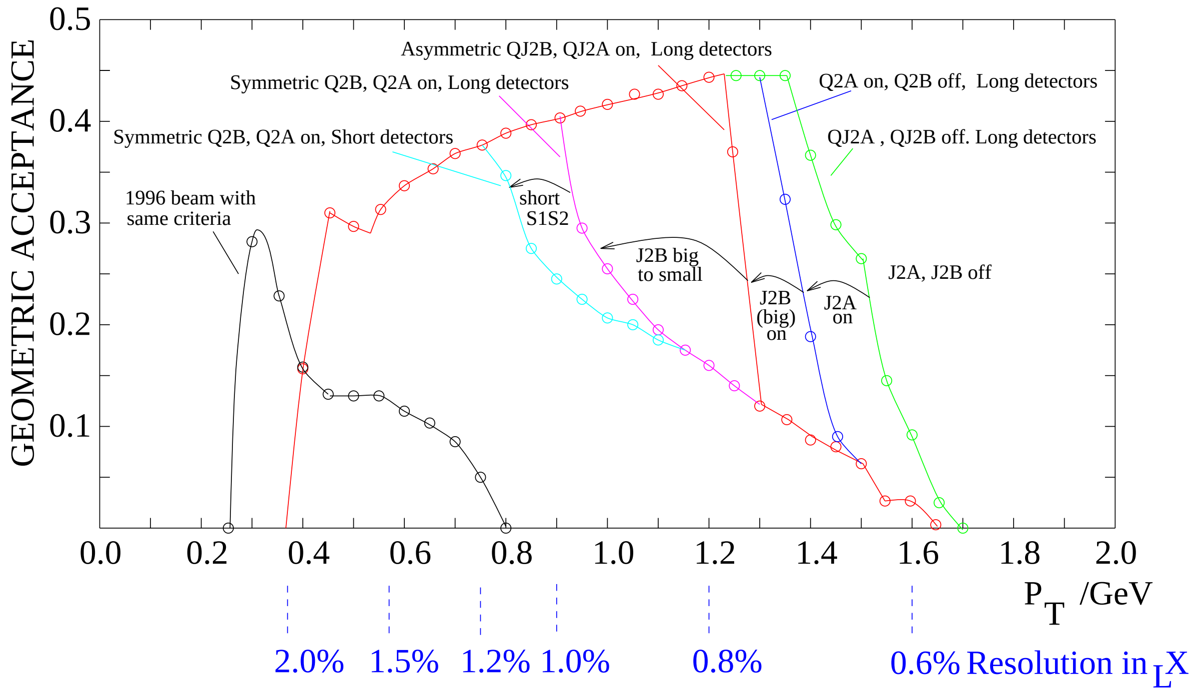

Figure 102: Showing the acceptance as a function of p_T for $x_L = 1.0$ for various geometrical assumptions. From left to right: the present spectrometer calculated with similar assumptions about detector distance from the beam; using present detectors and short horizontal arms on $QJ2B$; then using longer detectors for $S1$ and $S2$; then using longer detectors for $S1$ and $S2$ and using one lengthened side-arm on $QJ2B$. For reference, also the effect of switching off all vacuum restrictions at $QJ2B$ is shown and then the effect of switching off also the restrictions of $QJ2A$. The xL resolution varies across the detector. The second scale on the abscissa gives a rough indication of the x_L resolution for the updated version.

17 Summary